

## USING DISTRIBUTED CONTACTS IN DEM TO MODEL SHEAR FLOWS

Sharen J. CUMMINS<sup>1\*</sup> and Paul W. CLEARY<sup>2</sup>

<sup>1</sup> CSIRO Mathematical and Information Sciences, Clayton, Victoria 3169, AUSTRALIA

\*Corresponding author, E-mail address: sharen.cummins@csiro.au

### ABSTRACT

Granular flows in shear cells have been extensively studied using the Discrete Element Method (DEM) over the last two decades. These studies have typically been performed using the soft-sphere approach where deformation is assumed elastic and small relative to the characteristic grain scale. Consequently internal stresses and strains are not able to be modelled. As a first step towards addressing these limitations, we introduce a variant of DEM, the Distributed Contact DEM (DCDEM). This method models distributed normal and frictional contacts. In this initial implementation plastic deformation is not simulated and elastic deformation is simulated by permitting overlap as in traditional DEM. The method is compared against standard DEM for an oblique and normal impact and a granular shear cell in the small deformation limit.

### NOMENCLATURE

|       |                                       |
|-------|---------------------------------------|
| $C$   | damping coefficient (Ns/m)            |
| $ds$  | segment length (m)                    |
| $dx$  | overlap (m)                           |
| $F$   | force (N)                             |
| $J$   | moment of inertia ( $\text{kg m}^2$ ) |
| $k$   | spring stiffness (N/m)                |
| $m$   | mass (kg)                             |
| $Mo$  | moment (N m)                          |
| $N_g$ | number of grains                      |
| $N_p$ | number of points per grain            |
| $R$   | grain radius (m)                      |
| $t$   | time (s)                              |
| $\mu$ | dynamic friction coefficient          |
| $\nu$ | Poisson's ratio                       |
| $w_z$ | spin (rad/s)                          |

### INTRODUCTION

The Discrete Element Method (DEM) (Cundall and Strack 1979) is used extensively to model industrial and environmental granular flows (see for example Tsuji et. al, 1993, Mishra and Rajamani 1992, Xu and Yu 1997 and Cleary and Sawley, 2002). These examples employ a 'soft sphere' approach where grain overlaps are permitted and used in the contact force calculation. In these approaches, the local deformation is assumed small and any geometric change in shape of the grain does not need to be modelled. Typically elastic deformations must be restricted to 1.0% of a characteristic grain length scale in order to satisfy this small deformation limit. Contact forces are most commonly calculated using the linear spring-dashpot model (Walton 1983) with non-linear variants implemented by among others Zhou (Zhou et. al. 1999) and DiRenzo (DiRenzo et. al. 2004).

There are many granular flow problems we are motivated to model that traditional DEM cannot accurately model. An example is in tablet compression (Swarbrick and Boylan) and metal compaction (Cubberley et. al. 1983) under low pressures where the plastic deformation of individual particles (powders) represents the most important mechanism of densification. In these compaction applications cumulative grain deformation occurs due to successive inelastic collisions with other grains. The resulting shape change then alters further collisions. Traditional DEM assumes grain deformations are small and therefore does not incorporate the effect of geometric shape changes on the contact forces. Another example application that traditional DEM cannot model is in chemical mechanical polishing (Zhang, 1998). In this application the polishing pressure leads to plastic deformation of the surface. This in turn changes the contact area between the surface and the abrasive grains leading to altered frictional and adhesive forces. Similar issues arise in micro powder injection moulding (Schneider et. al. 2005) where the wear resistance of the mould inserts is important and dependant on the plastic deformation of the mould surface as well as the powder in the feed. Traditional DEM cannot capture such surface variations in the contact force calculations.

In this study we extend the DEM method to resolve the grain surface so that contact forces are calculated at discretised points along the grain surface. The method will in future be extended to allow for the calculation of finite grain deformations (such that the geometry of the grain alters). The scope of this paper, however, will be restricted to comparing the method in the low deformation limit where the traditional DEM approach is accurate.

Various numerical techniques have been extended to model contact between deformable bodies. In the finite element method (FEM) (Bandeira et. al 2004 and Kim et. al. 2008.), the contact constraint is formulated as a variational equation and solved using augmented Lagrangian or penalty methods. Additional elements are inserted at the contact surface to model finite deformation. In the boundary element method (BEM) (Simunovic and Saigal 1995 and Zhenan and Junping 2001), the boundary element equations are solved with a conforming discretisation of the surface to simulate moving contact of elastic bodies. In the smoothed particle hydrodynamics method (SPH) (Campbell et. al. 2000 and Seo et al 2008) elasto-plastic contact between spheres is modelled by solving a variational equation using a penalty method. Penetration between bodies is checked by calculating a penetration rate and the contact force is applied based on this penetration rate. In the material point method (MPM) (Bardenhagen et. al 2000) grains are modelled using a Lagrangian description in conjunction with an underlying

Eulerian grid to calculate interactions between them. Inter-granular contact is computed using an immersed boundary method which prevents interpenetration but allows sliding and separation.

The distributed contact DEM (DCDEM) presented here has similarities to the BEM in that only the grain surface is discretised (rather than the entire grain). Instead of solving the stress-strain equations at the discretisation points, a standard DEM contact force model is applied between interacting points on different grains. A given point on a given grain then has force contributions from nearby points on the other grain. In the following sections, the DCDEM method will be introduced and compared to traditional DEM for a 2D elastic oblique impact problem and a dense frictional granular flow under shear.

## DEM METHOD

In the DEM method grains are allowed to overlap, the amount of overlap,  $dx$ , normal  $v_n$  and tangential  $v_t$  relative velocities determine the collisional forces. For an inelastic collision, a linear spring-dashpot model is used to provide the normal force

$$F_n = -k_n dx + C_n v_n \quad (1)$$

and the tangential force is given by

$$F_t = \min(\mu F_n, k_t \int v_t dt + C_t v_t) \quad (2)$$

with the Coulomb limit being applied,  $dx$  is calculated using the known (unchanging) particle geometry and locations of the interacting grains.

## DISTRIBUTED CONTACT DEM MODEL

In DCDEM, pairs of interacting grains are first located using the standard DEM search algorithm. For a given pair of interacting grains,  $A, B$  we discretise the surface of each grain with a set of equi-spaced points. In this study, 2D simulations are employed and the grains are assumed to be circular. After the discretisation, grain  $A$  now has  $N_p$  equi-spaced points  $p_A^i$  located at  $\mathbf{r}_A^i = (x_A^i, y_A^i)$  on its surface. Each of these points is separated by a segment length  $ds_A$ . An analogous discretisation occurs for grain  $B$ . Refer to Figure 1. In this study we assume no change in connectivity of points on the grain.

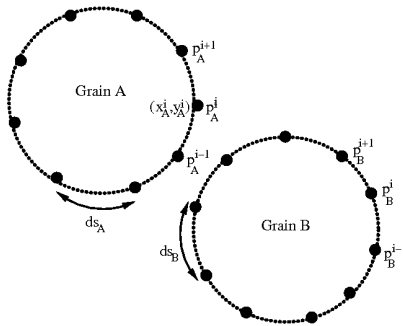


**Figure 1:** Discretisation of the grain surface with  $N_p$  points per grain.

For each point  $p_A^i$  store a set of neighbouring points  $H_A^i$ .

These neighbouring points are required in order to define a surface normal at  $p_A^i$ . For the 2D simulations in this study we choose

$$H_A^i = [p_A^{i-1}, p_A^i, p_A^{i+1}].$$

Repeat this process for grain  $B$ .

Consider now calculating the distributed forces for grain  $A$ . For each point  $p_A^i$  find points  $p_B^j$  on grain  $B$  such that

$$dr_{AB}^{ij} = |\vec{r}_A^i - \vec{r}_B^j| < ds_A.$$

If this condition is true a contact calculation may need to be performed between points  $p_A^i$  and  $p_B^j$ . Store all such  $p_B^j$  points in a list  $L_B$ . Refer to Figure 2.

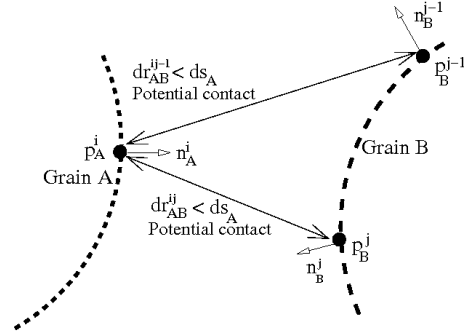


**Figure 2:** Checking for potential contacts between point  $p_A^i$  on grain  $A$  and nearby points on grain  $B$ . In this figure  $p_A^i$  has 2 potential contacts on grain  $B$ ,  $L_B = [p_B^{j-1}, p_B^j]$ .

If point  $p_A^i$  is involved in a potential contact, we need to calculate the outward surface normal at  $p_A^i$  in order to calculate contact forces. Rather than assuming knowledge of the surface shape in the region near  $p_A^i$  we instead use the neighbouring points of  $p_A^i$  to calculate an approximate normal,

$$\vec{n}_A^i = \frac{[-(y')_A^i, 1]}{\sqrt{(y')_A^i{}^2 + 1}} \quad (3)$$

where the gradient of the grain surface at  $p_A^i$  is

$$(y')_A^i = \frac{y_A^{i+1} - y_A^{i-1}}{x_A^{i+1} - x_A^{i-1}}.$$

For each point in  $L_B$ , calculate the normal in a similar way to Equation (3). For example, referring to the case in Figure 2,  $L_B = [p_B^{j-1}, p_B^j]$  therefore the following normals need to be calculated

$$\vec{n}_B^{j-1} = \frac{[-(y')_B^{j-1}, 1]}{\sqrt{(y')_B^{j-1}{}^2 + 1}} \quad \vec{n}_B^j = \frac{[-(y')_B^j, 1]}{\sqrt{(y')_B^j{}^2 + 1}}.$$

For point  $p_A^i$  we now have a list of potential contacting points associated with grain  $B$  stored in  $L_B$ . For each of these potential contacting points  $p_B^m$  in  $L_B$  we know the position and the normal vector. Calculate the overlap between points  $p_A^i$  and  $p_B^m$

$$dx_{AB}^{im} = (\vec{r}_A^i - \vec{r}_B^m) \cdot \vec{n}_A^i.$$

A contact between  $p_A^i$  and  $p_B^m$  will occur only when

$$dx_{AB}^{im} > 0.$$

In Figure 2 no contact occurs between  $p_A^i$  and  $p_B^j$  as the overlap  $dx_{AB}^{im} < 0$ .

For all points  $p_B^m$  in  $L_B$  with overlap  $dx_{AB}^{im} > 0$  calculate a distributed contact force and moment at point  $p_A^i$  using

$$\vec{F}_A^i = \frac{\sum_m \vec{F}_{AB}^{im} \alpha_{AB}^{im}}{\sum_m \alpha_{AB}^{im}} \quad Mo_A^i = \frac{\sum_m Mo_{AB}^{im} \alpha_{AB}^{im}}{\sum_m \alpha_{AB}^{im}}.$$

Here the weighting function  $\alpha^{im}_{AB}$  is a function of the angle between the normals at  $p^i_A$  and  $p^m_B$  and the overlap

$$\alpha^{im}_{AB} = \lambda \left( \bar{n}_A^i \cdot \bar{n}_B^m \mid dx^{im}_{AB} \right)$$

so that points aligned along the normal at  $p^i_A$  make a higher contribution to  $\bar{F}^i_A$  and  $Mo^i_A$ . In this study we employ

$$\lambda(q) = q^4 \quad (4)$$

so that contributions to the forces from points not aligned with the normal at  $p^i_A$  decay smoothly away. As the exponent increases the weighting function approaches a delta function and the results converge to DEM for *small overlaps*. Future work will involve investigating the nature and sensitivity of this weighting function to the results as grain geometry alters.  $\alpha^{im}_{AB}$  is an overlap measure at point  $p^i_A$  due to point  $p^m_B$ . We can define an overlap metric at point  $p^i_A$  as

$$\alpha^i_A = \sum_B \sum_m \alpha^{im}_{AB} \quad (5)$$

Figure 3 shows the normal force contributions to point  $p^i_A$  from points in  $L_B = [p^{j-1}_B, p^j_B]$ . These normal force contributions are denoted as  $F^{ij-1}_{n,AB}$  and  $F^{ij}_{n,AB}$  respectively. The contribution from  $p^{j-1}_B$  is weighted by the scalar  $\alpha^{ij-1}_{AB}$ . The contribution from  $p^j_B$  is weighted by the scalar  $\alpha^{ij}_{AB}$ . In this figure  $\alpha^{ij-1}_{AB} < \alpha^{ij}_{AB}$  as  $|\bar{n}_A^i \cdot \bar{n}_B^{j-1} \mid dx^{ij-1}_{AB} < |\bar{n}_A^i \cdot \bar{n}_B^j \mid dx^{ij}_{AB}$ .

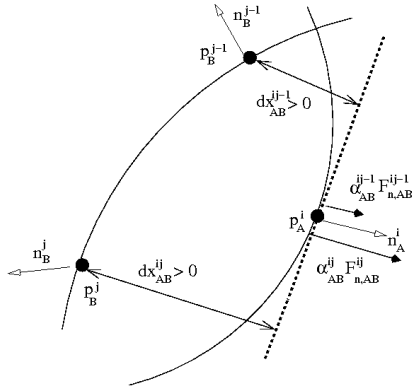


**Figure 3:** Normal force contributions to point  $p^i_A$  from nearby points  $p^{j-1}_B$  and  $p^j_B$

Each force contribution  $\bar{F}^{im}_{AB}$  is calculated using the DEM contact equations (1) and (2)

$$\bar{F}^{im}_{AB} = (F^{im}_{n,AB}, F^{im}_{t,AB}) \quad (6)$$

Each moment contribution is calculated using the tangential force  $\bar{F}^{im}_{t,AB}$  and the grain radius  $R_A$ ,

$$Mo^{im}_{AB} = R_A F^{im}_{t,AB} \quad (7)$$

We repeat the same process to find forces on all other points  $p^i_A$  on grain A and repeat for all other points on grain B. We then repeat for all other pair-wise grain interactions.

The forces on the grain vary along the grain surface, allowing for complex patterns of slip and no-slip as the Coulomb friction limit alters at every point. As the overlap increases (and the contact area increases) the DCDEM and DEM methods will diverge. This difference occurs because in two-dimensional DEM grains deform and contact along a line. Traditional DEM accounts for

this deformation so that the normal force is analytically correct. In DCDEM the surface force varies across a curved contact area that does not (currently) deform. Therefore, the normal force in DCDEM will only be analytically correct when a single contact point occurs in the collision. This rigid grain assumption is a limitation of the current DCDEM method and will be addressed in further development.

To model the grains as rigid bodies, the points on grain A translate with a uniform grain velocity,  $v_A$  and have a uniform spin  $w_A$  around the center of the grain. This velocity is found by summing the forces  $\bar{F}^i_A$  on the points belonging to grain A and dividing through by the grain mass  $m_A$

$$\bar{v}_A(t+dt) = \bar{v}_A(t) + \frac{dt}{m_A} \sum_i \bar{F}_A^i$$

Similarly, the rigid spin is calculated by summing the moments  $Mo^i_A$  on the points on grain A and dividing through by the grain's moment of inertia  $J_A$

$$\bar{w}_A(t+dt) = \bar{w}_A(t) + \frac{dt}{J_A} \sum_i Mo^i_A$$

## OBLIQUE IMPACT

For the first comparison of DCDEM, we examine the frictional oblique impact of two elastic steel grains. This problem has been studied extensively in the literature, see for example Wu (2001), Thornton et. al (2001) and Di Renzo et.al (2004). Figure 4 displays the configuration. In this study  $\mu = 0.1$ ,  $R = 50$  mm. We study two impact angles,  $\theta = 10^\circ$  and  $\theta = 0^\circ$ . The material properties of the steel points are given in Table 1. A spring stiffness of  $k_n = 8$  MN/m is used to ensure overlaps in the traditional DEM are very small. The time step is chosen such that the collision takes 200 time steps. The simulation is run for 0.008 s to model the complete collision. In the DCDEM simulation each grain has  $N_p = 150$  points.

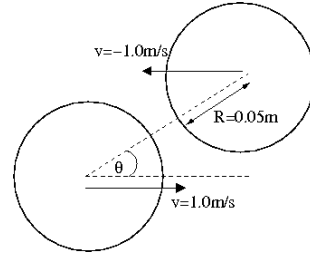


**Figure 4:** Configuration for the oblique impact problem.

| E      | $\nu$ | $\rho$                 |
|--------|-------|------------------------|
| 70 GPa | 0.3   | 7850 kg/m <sup>3</sup> |

**Table 1:** Material properties of steel grains used in the oblique impact problem.

## OBLIQUE IMPACT, $\theta = 10^\circ$

Figure 5 and Figure 6 show snapshots of the collision using the DCDEM and DEM methods at 5 ms and 8 ms respectively. We denote the blue grain as grain 1 and the grey grain as grain 2.

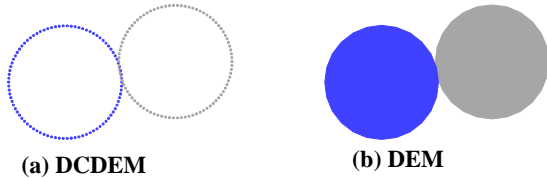


**Figure 5:** Grain positions at  $t = 5$  ms for (a) DCDEM and (b) DEM methods.

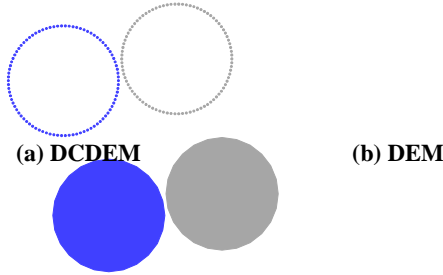


**Figure 6:** Grain positions at  $t = 8$  ms for (a) DCDEM and (b) DEM methods.

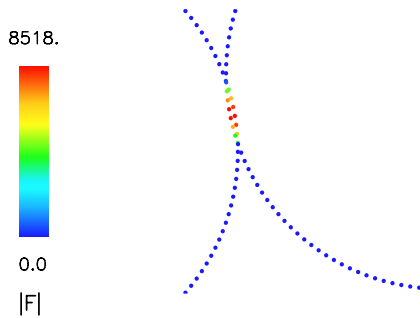


**Figure 7:** Force variation (in Newtons) along the contacting surfaces at  $t = 4$  ms for the DCDEM method.

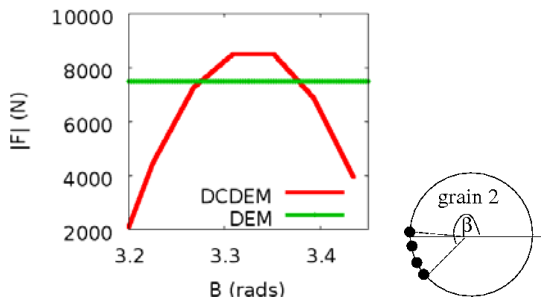


**Figure 8:** Force variation at the contacting points along the surface of grain 2 at  $t = 4$  ms for DCDEM and DEM methods. The value along the horizontal axis represents the radian value at each contacting point on grain 2 as shown in the schematic diagram on the right.

Figures 7 and 8 show the spatial variation in the force along the contacting surfaces at 4 ms for DCDEM and DEM. They highlight the difference between the two methods. In DCDEM the force varies along the curved contacting surface (as the overlap, tangential displacement and Coulomb friction limit vary) while in DEM the force is applied along a linear contact line and assumed constant along this line. The spring stiffness is relatively large leading to a small overlap. As a result a maximum of 7 points on grain 2 are in contact with grain 1 during the collision. We found the shape of the DCDEM surface

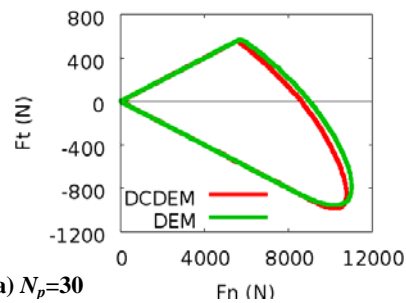
force graph in Figure 8 is dependant on the choice of weighting function in Equation (4). As the exponent in Equation (4) increases, the maximum surface force decreases (as points on grain A are influenced by fewer points on grain B) and the results approach traditional DEM.

We compare the contact forces during the collision for the two methods. Specifically, we measure normal force versus tangential force throughout the collision. For the DCDEM, we integrate the normal and tangential forces along the contacting surface area. The contacting surface will contain points with a non-zero overlap measure  $d_A^i$  (defined in Equation 5). Therefore the forces are weighted by  $\alpha_A^i$  in the integration. The resulting volume integral approximates the work done on grain A. This volume integral is then normalised to obtain the collision forces. For grain A these collision forces are

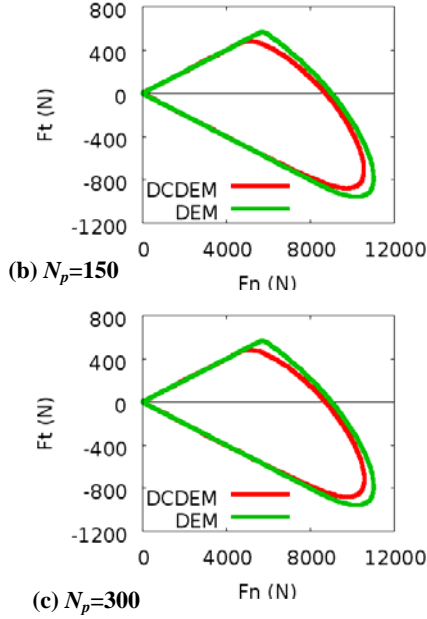
$$\vec{F}_A = (F_{nA}, F_{tA}) = \frac{\int \vec{F}_A^i \alpha_A^i ds_A}{\int \alpha_A^i ds_A} \quad (5)$$

Figure 9 shows plots of the normal force versus tangential force using the DEM and DCDEM methods for grain 2 (the grey grain shown in Figures 5 and 6). Results are shown for  $N_p = 30$  (Figure 9a),  $N_p = 150$  (Figure 9b) and  $N_p = 300$  points (Figure 9c). Grain 2 first begins in the sliding regime with an increasingly negative tangential force. When the normal force increases to  $F_n \sim 10000$  N and the tangential force  $F_t \sim -1000$  N, the Coulomb friction limit is no longer reached and the grain stops sliding. During this phase, the normal force decreases as the grain unloads and the tangential force changes sign. When the normal force reduces to  $F_n \sim 6000$  N, the Coulomb limit is once again satisfied and sliding resumes during the remainder of the collision. The collision can therefore be characterised as having an initial sliding phase, an unloading phase and a final sliding phase.

Figure 9 shows that as the number of points increase the results do not converge toward the traditional DEM results for this particular spring stiffness. At  $N_p = 30$ , the comparison is excellent because only 2 contacting points on grain 2 occur in the collision. The contact region is close to linear as is the case in traditional DEM. As the resolution increases and more points are involved in the collision, differences are noted in the normal force at the end of the loading phase. The DCDEM results suggest an effective spring stiffness less than DEM. The differences occur because the contact area is now a curved surface (see Figure 7) and the forces vary along this surface, in contrast to traditional DEM.



**(a)  $N_p=30$**



**Figure 9:** Normal versus tangential forces on grain 2 during the oblique impact using DCDEM (red) and DEM (green) for (a)  $N_p=30$ , (b)  $N_p=150$  and (c)  $N_p=300$  points.

#### NORMAL IMPACT, $\theta = 0^\circ$

To quantify the errors in DCDEM we investigate a normal impact ( $\theta=0^\circ$ ). For a two-dimensional elastic normal impact, the normal force varies linearly with grain overlap. In this problem grain overlap is defined as

$$dx_{AB} = (Xcom_A - Xcom_B) - (R_A + R_B)$$

where  $Xcom_A$  is the  $x$  coordinate of the centre-of-mass position of grain  $A$ . We ran the DCDEM simulations using  $N_p=50$ ,  $N_p=300$  and  $N_p=900$ . Figure 10 shows the results. Traditional DEM exhibits a linear contact force law and reproduces the correct spring stiffness. DCDEM shows a linear law up to  $N_p=300$ . The correct spring stiffness is reproduced using  $N_p=50$ . This is not surprising since at this low resolution only a single contact point is involved in the collision. As the resolution increases to  $N_p=300$  the spring stiffness is less than the analytical result by approximately 9%. At  $N_p=900$  the error remains at approximately 9%. However the results deviate from the linear law with small jumps in the force occurring due to additional contact points intermittently entering the support of the weighting function. At these higher resolutions more points are involved in the calculation of a given point's contact force. Further work is required in the numerical algorithm to ensure forces vary smoothly as the region of influence on a given contact point alters. In addition errors result because the contact area is a curved surface and the force varies along this surface (rather than being constant along a straight contact line as is analytically correct).

These two impact problems highlight a limitation in verifying DCDEM when the contact area in DCDEM contains multiple points and the grains are assumed rigid. For artificially soft springs, the overlaps and the contact areas increase producing differences regardless of the numerical resolution. Grain deformation needs to be

incorporated in DCDEM in order to perform validation for softer springs.

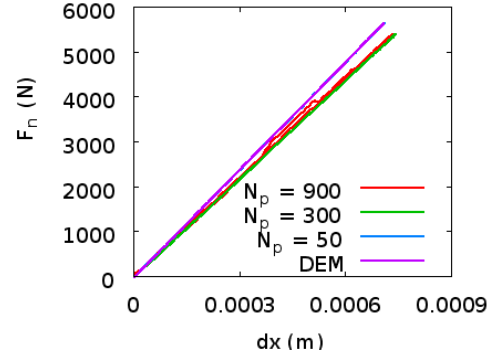


**Figure 10:** Normal force versus grain overlap for DCDEM using  $N_p=50$ ,  $N_p=300$  and  $N_p=900$  points compared against traditional DEM.

#### 2D SHEAR CELL

Granular shear flows have been well investigated with studies on the effect of boundary conditions (Campbell 1987, 1993), particle size and shape (Cleary, 2008). For the second verification, we simulate such an inelastic granular shear flow using both DEM and DCDEM, using a coefficient of restitution  $e_n = 0.8$  and friction coefficient  $\mu = 0.5$ . A spring stiffness of  $k_n=0.5$  MN/m is used. In traditional DEM this spring stiffness is large enough to ensure overlaps are small. Given the results from the previous section, we expect this artificially soft spring will produce differences in the collisional forces between DCDEM and DEM. We are motivated then to compare how such differences influence the flow characteristics in the shear cell.

Figure 11 shows the computational configuration. The shear cell is a unit square with top and bottom walls moving at  $v = 0.5$  m/s and  $v = -0.5$  m/s respectively. Periodic boundaries are applied at the left and right edges. A grain radius  $R = 0.02$  m is used and an initial volume fraction  $V_f = 0.5$  is chosen (which has 357 grains). In the DCDEM simulation we use  $N_p=90$ . The time step was chosen such that a minimum of 15 time steps are used to resolve each collision. Table 2 provides the material properties of the grains.

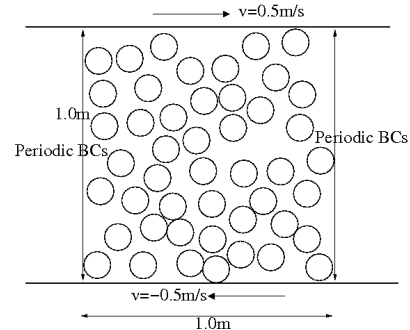
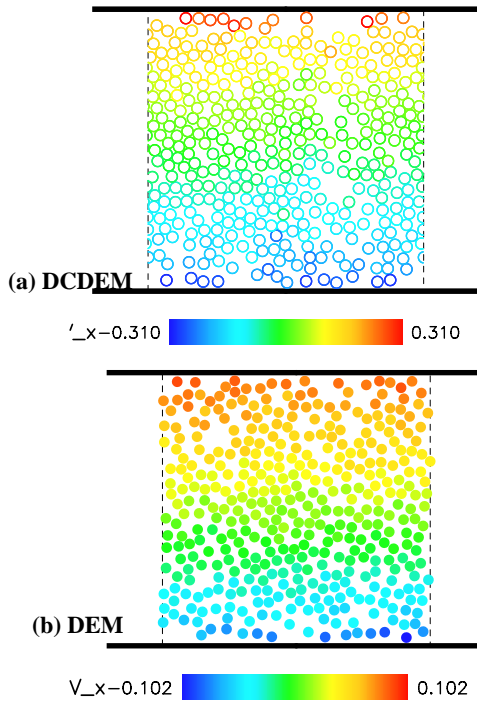


**Figure 11:** Configuration for the 2D shear cell problem.

| E      | $\nu$ | $\rho$                 |
|--------|-------|------------------------|
| 70 GPa | 0.3   | 1000 kg/m <sup>3</sup> |

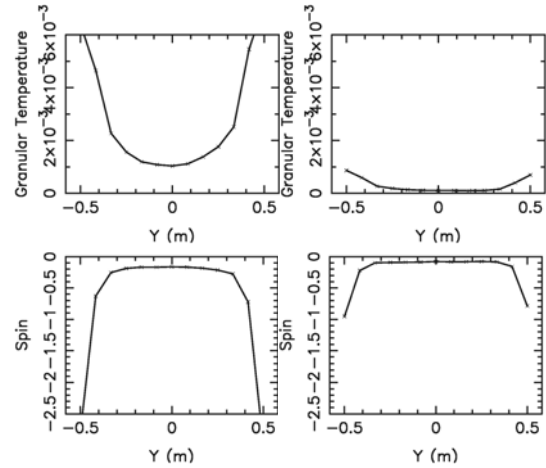
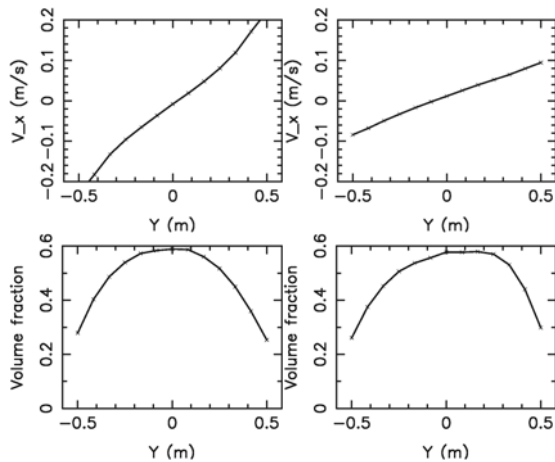
**Table 2:** Material properties of the grains used in the shear cell problem.

The simulation was run until a steady state was reached at time  $t = 400$  s. Figure 12 shows the grain distribution coloured by stream-wise velocity at  $t = 400$  s for DCDEM (Figure 12a) and DEM (Figure 12b).



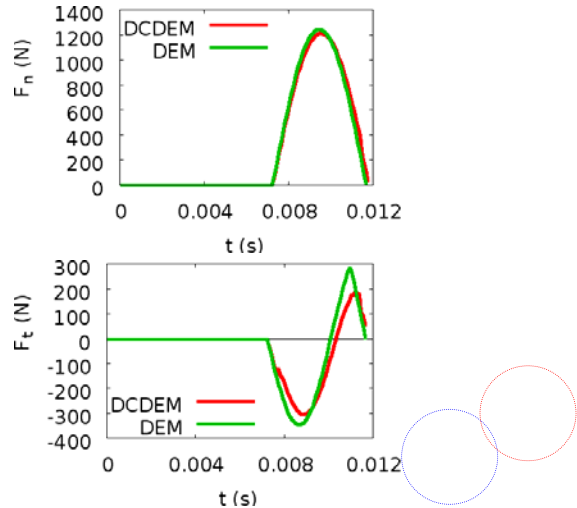
**Figure 12** Grain positions in the shear cell at time  $t = 400$  s for (a) DCDEM and (b) DEM.

Figure 13 shows the average flow characteristics at  $t = 400$  s for DCDEM (left column in Figure 13) and DEM (right column in Figure 13). The characteristics are averaged spatially (Cleary, 2008). Stream-wise velocity ( $V_x$ ), granular temperature, volume fraction and spin are shown for both methods. As expected the flow characteristics differ between the two methods. Use of the distributed contacts causes larger stream-wise velocities, granular temperatures and spins near the walls. It has a minor impact on the volume fraction.



**Figure 13** Flow characteristics in the shear cell at time  $t = 400$  s for DCDEM (left column) and DEM (right column).

We suspect the differences in these flow characteristics are due to the artificially soft spring stiffness  $k_n=0.5$  MN/m which lead to significant contact areas in the DCDEM simulation. To test this we modelled an oblique impact with the same numerical parameters used in this shear cell and measured collisional forces. Figure 14 shows the normal and tangential force comparisons during the collision using  $k_n=0.5$  MN/m. The figure also shows the grain positions in DCDEM at the time of highest overlap. The normal force comparisons between DCDEM and DEM are within 1%. However the tangential force comparisons show approximately 30% difference in the peak, with DCDEM predicting a smaller tangential force. The grain overlap is significant too leading to approximately 10% of the grain surface in contact.



**Figure 14** Normal ( $F_n$ ) and tangential ( $F_t$ ) forces for DCDEM and DEM during an oblique impact test for impact angle  $\theta = 20^\circ$  with  $k_n = 0.5$  MN/m. The grain positions at maximum overlap are shown on the right.

Figure 14 highlights that DCDEM cannot be used with an artificially soft spring when the grains are assumed rigid. The contacting surface deviates significantly from the linear surface in traditional DEM which changes the collisional forces and dynamics producing the differences seen in the shear cell. At this spring stiffness it is imperative to model grain deformation with DCDEM.

## CONCLUSION

The DCDEM method is an extension of the traditional DEM method involving calculation of contact forces at discretised points along the surface of a grain. By resolving the grain surface, the method has the potential to model surface force variation during the collision. A current limitation of the method is that grain deformation is not simulated. This has meant that verification of DCDEM is currently restricted to comparisons against traditional DEM for stiff springs where the contact area is small. This study has shown that the use of artificially soft springs with rigid grains produce curved contact areas in DCDEM. For these soft springs, results for the DCDEM deviated from theory and from traditional DEM. These differences were noted in the shear cell simulation. Further testing of the model needs to be performed to ascertain if it is the nature of the contact area which alters the collisional forces and grain dynamics and/or an algorithmic issue associated with how the forces are calculated at each contact point.

Combining the DCDEM method with grain deformation is the next developmental step. This will allow for the modelling of inter-granular collisions undergoing plastic deformation, broadening the range of granular flow problems that can be simulated as well as allowing for further validation.

## REFERENCES

- BANDEIRA, A.A., WRIGGERS P. and PIMENTA P., (2004), "Numerical derivation of contact mechanics interface laws using a finite element approach for large 3D deformation", *Int. J. Numer. Meth. Engng.*, **59**, 173-195.
- BARDENHAGEN, S.G., BRACKBILL, J.U. and SULSKY D., (2000), "The material-point method for granular materials", *Comput. Meth. Appl. Mech. Eng.* **187**, 529.
- CAMPBELL, C.S. and GONG, A. (1987), "Boundary conditions for two-dimensional granular flows", *Proc. Sino-US Symposium on Multiphase Flow, Hangzhou, China*, **1**, 278-283.
- CAMPBELL, J., VIGNJEVIC, R. and LIBERSKY, L., (2000), "A contact algorithm for smoothed particle hydrodynamics", *Comput. Method Appl. Mech. Eng.*, **184**, 49-64.
- CLEARY, P.W. (2008), "The effect of particle shape on simple shear flows", *Powder Technology*, **179**, 144-163.
- CLEARY, P.W. and SAWLEY, M.L., (2002), "DEM modelling of industrial granular flows: 3D case studies and the effect of particle shape on hopper discharge", *Appl. Math. Modelling*, **26**, 89-111.
- CUBBERLEY, W.H. and BACKERJIAN, R., (1983), "DESK ADDITION: Tool and Manufacturing Handbook", *Society of Manufacturing Engineers*.
- CUNDALL, P.A. and STRACK, O.D.L., (1979), "Discrete numerical model for granular assemblies", *Geotechnique*, **29**, 47-65.
- KIM, J.H., LIM, J. H., LEE, J.H. and IM, S., (2008), "A new computational approach to contact mechanics using variable-node finite elements", *Int. J. Numer. Meth. Engng.*, **73**, 1966-1988.
- MISHRA, B.K. and RAJAMANI R.J., (1992), "The discrete element method for the simulation of ball mills", *Appl. Math. Modelling*, **16**, 598-604.
- SCHNEIDER. J., IWANEK. H. and ZUM GAHR. K.H., (2005), "Wear behaviour of mould inserts used in micro powder injection moulding of ceramics and metals", *Wear*, **259**, 1290-1298.
- SEO, S., MIN, O. and LEE, J., (2008), "Application of an improved contact algorithm for penetration analysis in SPH", *Int. Journal of Impact Engineering*, **35**, 578-588.
- SIMUNOVIC, S. and SAIGAL, S., (1995), "Contact Surface Optimization Using Boundary Element Method", *Computers and Structures*, **56**, 745-750.
- SWARBRICK, J. and BOYLAN J. (2002), "Encyclopedia of Pharmaceutical Technology", 2<sup>nd</sup> edition, Volume 3.
- TSUJI, Y., TANAKA T. and ISHIDA T., (1992), "Lagrangian numerical simulation of plug flow of cohesionless particles in a horizontal pipe", *Powder Technol.*, **71**, 239-250.
- XU, B.H. and YU, A.B., (1997), "Numerical simulation of the gas-solid flow in fluidized bed by combining discrete particle method with computational fluid dynamics", *Chemical Engineering Science*, **52**, 2785-2809.
- WALTON, O.R., (1983), "Mechanics of granular materials", *Jt Kenkins and M Satake, eds, Elsevier*, 327-338
- ZHANG, F. and BUSNAINA A., (1998) "The Role of Particle Adhesion and Surface Deformation in Chemical Mechanical Polishing Processes", *Electrochem. Solid-State Lett.*, **1**, 184-187.
- ZHENHAN, Y. and JUNPING, P. (2001), "Boundary Element Method for Moving and Rolling Contact of 2D Elastic Bodies with Defects", *Acta Mechanica Sinica*, **17**, 183-192.